Bulletin de la Socié Royale des Sciences de Liège - Vol. 74, 1-2-3, 2005, pp. 79-95

Observations of Active Galactic Nuclei with Next Generation Optical Interferometers

Alessandro Marconi*
INAF-Osservatorio Astrofisico di Arcetri, Firenze, ITALY

Abstract: Next Generation Optical Interferometers with a spatial resolution of 0.1 mas in the K band will lead to major steps forward in our understanding of Active Galactic Nuclei. In this paper, I will show how they can be used to study the morphology of the obscuring torus, the geometry and kinematics of the Broad Line Region, Supermassive Black Holes in galactic nuclei and the cosmological evolution of their relations with the host galaxies.

1 Introduction

Active Galactic Nuclei (AGN) are galactic nuclei showing evidence for non-stellar production of energy. The most stringent constraints on the energy production mechanism come from the emitted luminosities (L$\sim 10^8 - 10^{13}$L$_\odot$), the flat ($L_\nu \sim \nu^{-1}$) non-stellar spectra extending from radio to γ-rays, the high efficiencies of matter-energy conversion ($\simeq 0.1$), the rapid time variabilities (observed on scales as short as a few hours in optical and X-rays), the compact source sizes (directly measured in radio sources and smaller than a few light days) and the presence of relativistic jets (e.g. Blandford, Netzer & Woltjer 1990). Observationally all AGNs can be roughly divided into two main classes, type 1 and type 2 (e.g. Seyfert 1 and 2 nuclei). The type 1 AGNs show broad ($FWHM > 1000$ km/s) permitted emission lines in their optical and near-IR spectra while type 2 AGNs only show narrow permitted lines ($FWHM < 1000$ km/s). The most widely accepted model comprises a central black hole with mass in the range $10^6 - 10^{10}$M$_\odot$ surrounded by an accretion disk that converts gravitational energy into radiation and outflows (see Fig. 1). The radiation emitted in the optical – UV – soft X-rays accounts for most of the AGN bolometric luminosity. Broad emission lines originate in small high density gas clouds ($N_{\rm e} \sim 10^9$ cm^{-3}) orbiting around the nuclear source. Variability time scales of the broad line fluxes and other theoretical arguments suggest that the Broad Line Region (BLR) size ranges from a few light days for nearby Seyfert 1 galaxies up to a few light years in the most luminous quasars. Plasma jets are emitted perpendicularly to the disk. At large radii ($\sim 1 - 100$ pc), an obscuring torus of cold gas and dust surrounds the nucleus. The orientation of this torus relative to the line of sight naturally accounts for the differences between type 1 and type 2 AGNs (see Fig. 1 and Antonucci 1993 for a review) because in type 2 AGNs the BLR is hidden from direct view and only narrow lines emitted from the Narrow Line Region (NLR) are seen in spectra.

*email: marconi@arcetri.astro.it

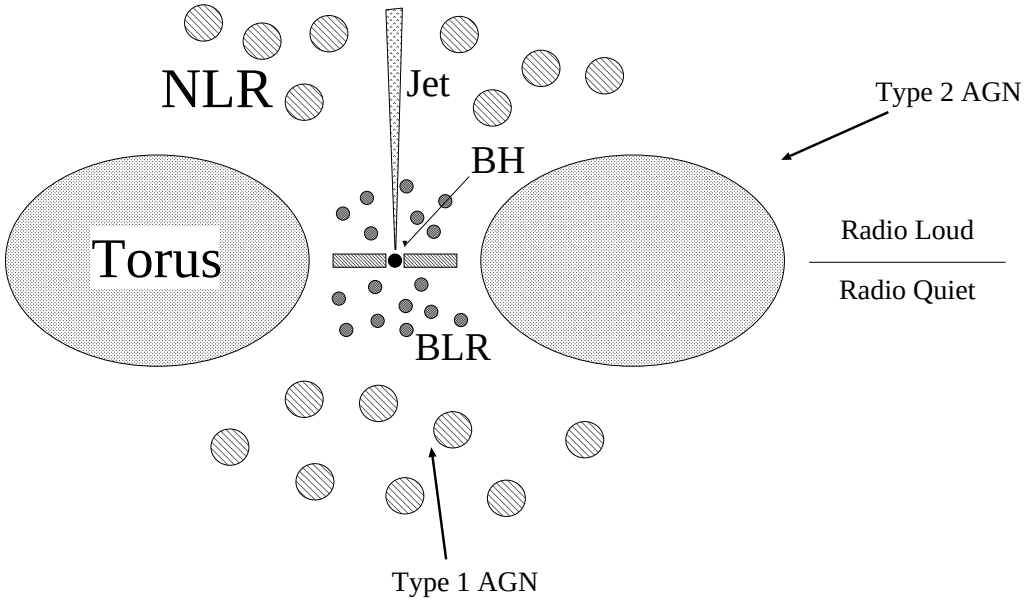

Figure 1: Schematic view of the unified model for AGNs. The components are not drawn in scale. The BLR (Broad Line Region) size ranges from a few light days in local Seyfert 1 galaxies to a few light years in bright quasars. Similarly the obscuring torus size ranges from ~ 1 to ~ 100 pc. Finally the NLR (Narrow Line Region) can range from ~ 100 pc up to several Kpc.

2 Spatial Scales of AGN Components

After the brief introduction in the previous section, we summarize the relevant spatial scales of the various AGN components in order to select the targets which could be observed with Next Generation Optical Interferometers (hereafter NGOI). According to the unified model, the main components of an AGN are:

Narrow Line Region	$R_{\rm NLR} \sim 1600 \left(\frac{L}{10^{12} L_\odot}\right)^{0.6}$ pc
Obscuring Torus	$R_{\rm Dust\ Subl.} \sim 0.1 - 2.5 \left(\frac{L}{10^{12} L_\odot}\right)^{0.5}$ pc
Radio Jet	from sub–pc to kpc–scales
Broad Line Region	$R_{\rm BLR} \sim 0.1 \left(\frac{L}{10^{12} L_\odot}\right)^{0.7}$ pc
Accretion Disk	$R_{\rm Disk} \sim 0.03 \left(\frac{T}{1000{\rm K}}\right)^{-4/3} \left(\frac{M}{10^8 M_\odot}\right)^{1/3} \left(\frac{L}{10^{12} L_\odot}\right)^{1/3}$ pc
Black Hole	$R_{\rm Schwarzschild} = 4.8{\times}10^{-6} \left(\frac{M}{10^8 M_\odot}\right)$ pc
	$R_{\rm BH} = 12.4 \left(\frac{M}{10^8 M_\odot}\right)^{0.5}$ pc

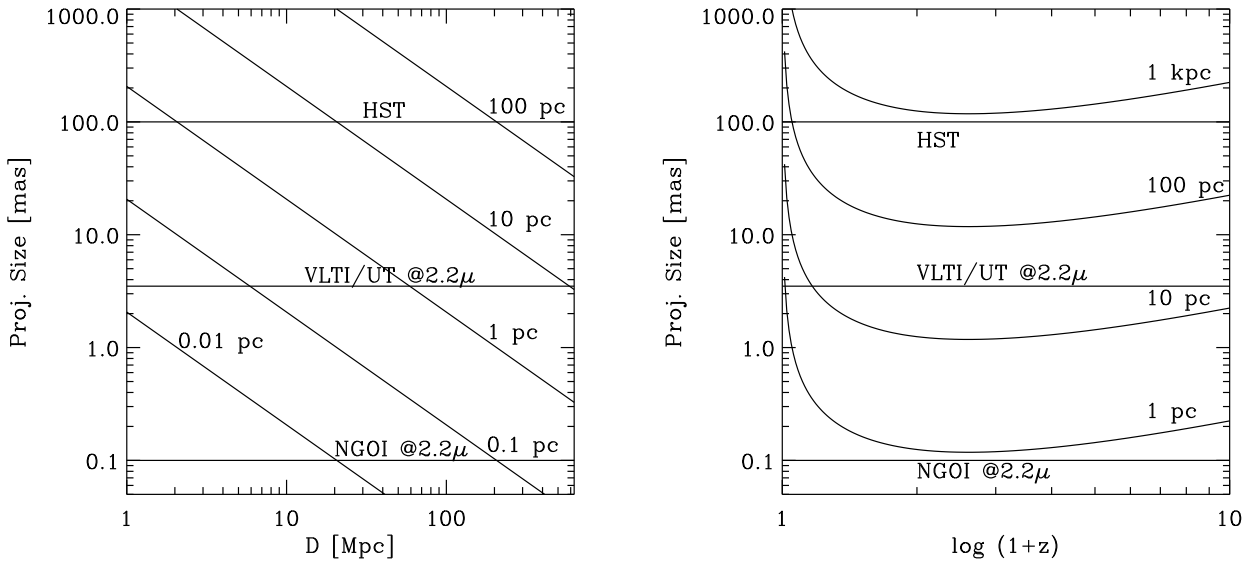

Figure 2: Projected physical scales on the plane of the sky in the local universe (left) and in the $z = 1 - 10$ range (right). For comparison we show the spatial resolutions of HST, VLTI and NGOI.

The size of the NLR, $R_{\rm NLR}$ is taken from Schmitt et al. (2003) and from Bennert et al. (2002) who provide an observational relation between $R_{\rm NLR}$ and [OIII]λ 5007Å luminosity. Using known [OIII]/Hβ ratios, the Hβ-$L_{\rm B}$ relation (Ho & Peng 2001) and the bolometric correction $L/\nu_{\rm B}L_{\rm B} = 7$ (e.g. Marconi et al. 2004) one can derive the scaling relation between $R_{\rm NLR}$ and AGN bolometric luminosity L.

A typical size of the obscuring torus in the near infrared is given by the dust sublimation radius $R_{\rm Dust\ Subl.}$, i.e. the radius at which dust is sublimated by the UV AGN continuum. The range of values shown above are from Laor & Draine (1993) and reflect different possible dust compositions.

The size of the BLR, estimated with reverberation mapping (see below), is taken from Kaspi et al. 2000 after converting B band continuum luminosity to bolometric luminosity. Note that, as suggested by Netzer & Laor (1993), the BLR outer boundary could be set by the dust sublimation radius.

For the size of the accretion disk we have considered the radius at which the disk reaches $T \sim 1000\,{\rm K}$ and emits mostly in the near infrared. The formula for $R_{\rm Disk}$ is obtained with a standard Shakura & Sunyaev α-disk but is an-over simplification accurate only for order of magnitude estimates (see Shapiro & Teukolsky 1983 for more details).

For the Black Hole (BH) we show the classical Schwarzschild radius and the radius of the BH sphere of influence. This is defined as $R_{\rm BH} = GM_{\rm BH}/{\sigma_\star}^2$, where $\sigma_\star$ is the galaxy stellar velocity dispersion, and roughly represents the radius at which the gravitational potentials of BH and stars are comparable. $\sigma_\star$ has been removed by using the $M_{\rm BH}$-$\sigma_\star$ relation with the coefficients by Tremaine et al. 2002.

Band	J	H	K
		$\mathcal{R} = 35$	
VLTI+AMBER	18.5	20.2	19.8
NGOI	21	23	22
		$\mathcal{R} = 1000$	
VLTI+AMBER	14.4	16.6	17.4
NGOI	17	19	20

Table 1: Expected performances of VLTI+AMBER compared with those of NGOI. The expected VLTI+AMBER limiting magnitudes are for a 5σ detection in 4 h integration time with average seeing ($0.65''$) and fringe tracking. NGOI limiting magnitudes are derived assuming that it can go deeper by a factor ten in flux.

3 Desirable Characteristics of Next Generation Optical Interferometers and Possible AGN Science Cases

We define here the basic characteristics of Next Generation Optical Interferometers (NGOI) which are desirable for significant step forward in our understanding of AGN phenomena, starting from what is currently possible with the VLTI (see, for instance, Marconi et al. 2003). AGN studies with the VLTI are currently limited to the UTs, thus it is possible to obtain only a few visibility points in the *uv* plane without imaging capabilities. NGOI should provide full imaging capabilities and, since the scientific goals described below do not require instantaneous imaging, aperture synthesis with image reconstruction is acceptable. Like the VLTI, NGOI should spectrally disperse fringes with a low ($\mathcal{R} \sim 100$) and medium resolution mode ($\mathcal{R} \sim 1000 - 2000$). Considering only UTs, the VLTI has a 3 mas resolution in the K band; NGOI should achieve a resolution of 0.1 mas in K (i.e. a maximum baseline of ~ 4 km). Finally the VLTI has a moderate sensitivity and the expected overall efficiencies in J, H and K of the VLTI with AMBER are of the order of 2-3%; with NGOI it should be possible to improve the sensitivity by at least a factor 10. In Table 1 we compare the expected performances of the VLTI+AMBER with those of NGOI which are assumed to go a factor 10 deeper in flux.

We now compare the desirable spatial resolution of NGOI (0.1 mas in K) with the spatial scales of the AGN components outlined in the previous section. In Fig. 2 we show how spatial scales are converted to projected scales on the plane of sky in the local universe (left) and up to high redshift (right). We have assumed standard values for the cosmological parameters, i.e. $H_0 = 70\,\mathrm{km\,s^{-1}\,Mpc^{-1}}$, $\Omega_\mathrm{M} = 0.3$ and $\Omega_\Lambda = 0.7$. It is clear that the NLR is too big and can be studied with conventional telescopes, while the accretion disk in the near-infrared and the Schwarzschild radius are too small. Apart for the jet, which is already studied at radio wavelengths, we can study 3 important AGN components namely the Obscuring Torus, the Broad Line Region and the Black Hole (in the sense of detecting its presence and measuring its mass).

4 The Supermassive Black Hole

According to the unified model, all AGNs are powered by accretion of matter onto massive BHs. This belief, combined with the observed evolution of the space density of AGNs (Soltan 1982, Marconi et al. 2004) and the high incidence of low-luminosity nuclear activity in nearby galaxies implies that a significant fraction of luminous galaxies must host a BH of mass ($M_{\rm BH} \simeq 10^6 - 10^{10} M_\odot$) in their nuclei. In recent years BHs have been detected and their masses measured in ~ 40 galaxy nuclei, both normal and active (e.g. Kormendy & Gebhardt 2001, Ferrarese & Ford 2004). It has also been found that a tight correlation exists between the BH mass and host bulge (spheroid) mass and luminosity (e.g. Kormendy & Richstone 1995, Marconi & Hunt 2003) and with the stellar velocity dispersion (Ferrarese & Merritt 2000, Gebhardt et al. 2000). Clearly any correlation of the BH and spheroid properties implies a tight relation between galaxy and BH formation.

By far, the best evidence for a BH in a galactic nucleus is given by center of our own Galaxy where, given the relatively small distance ($D \simeq 8$ kpc), it has been possible to measure proper motions and radial velocities of many stars thus directly probing the gravitational field (e.g. Genzel et al. 2000, Schödel et al. 2003). In the case of one star it has been possible to follow almost completely its elliptical orbit around the putative BH over more than 10 years of observations (e.g. Ghez et al. 2000, Schödel et al. 2003). The dark object responsible for the gravitational attraction and coincident with the radio source Sgr A* must have a mass of $M_\bullet \simeq 3{\times}10^6 {\rm M}_\odot$ and a mean density of at least $\rho_{\rm BH} > 10^{17} {\rm M}_\odot\,{\rm pc}^{-3}$. Clearly, the only plausible alternative is that of a supermassive Black Hole.

The second best case for a supermassive BH is given by NGC 4258, where high spatial resolution VLBI observations of H_2O maser emission imply the presence of a dark mass of $\simeq 4{\times}10^7 {\rm M}_\odot$ concentrated within a radius of 4 mas (0.14 pc) implying $\rho_{\rm BH} > 4{\times}10^9 {\rm M}_\odot\,{\rm pc}^{-3}$ (Miyoshi et al. 1995). Also in this case the most plausible alternative is that of a BH even if the evidence is not as strong as for our Galactic Center BH.

The evidence for a BH in all cases other than the Galactic Center and NGC 4258 is much weaker due to the worse spatial resolution of the observations. To detect a BH one must resolve the radius of the BH sphere of influence:

$$R_{\rm BH} = \frac{G M_{\rm BH}}{{\sigma_\star}^2} = 4.3\,{\rm pc} \left(\frac{M_{\rm BH}}{10^7 {\rm M}_\odot}\right) \left(\frac{\sigma_\star}{100\,{\rm km\,s^{-1}}}\right)^{-2} \quad (1)$$

which projected on the plane of the sky is

$$\theta_{BH} = 0.1'' \left(\frac{M_{\rm BH}}{10^7 {\rm M}_\odot}\right) \left(\frac{\sigma_\star}{100\,{\rm km\,s^{-1}}}\right)^{-2} \left(\frac{D}{10\,{\rm Mpc}}\right)^{-1} \quad (2)$$

It is clear that in order to probe the BH sphere of influence high spatial resolution is mandatory. Until now, except for the Milky Way and NGC 4258, the best spatial resolution achievable is given by HST, i.e. $\sim 0.1''$. BH are usually detected and their mass measured with gas kinematics (e.g. Marconi et al. 2001, Barth et al. 2001, Marconi et al. 2003 and references therein) or stellar dynamics (e.g. Gebhardt et al. 2003, Verolme et al. 2002 and references therein). What is really measured from observations of either gas or stellar kinematics is the amount of dark mass needed to explain the observed motions. If this dark mass is pointlike at the resolution of the observations then it is a BH candidate and is usually called a Massive Dark Object

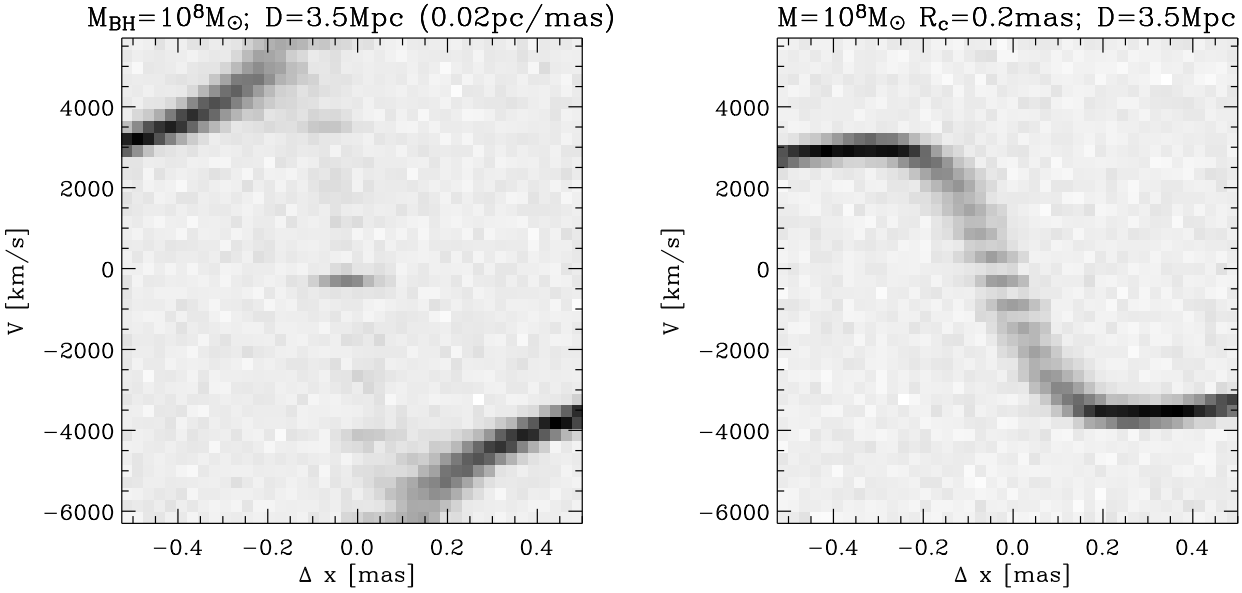

Figure 3: Position velocity diagrams from NGOI observations of Centaurus A ($D = 3.5\,\mathrm{Mpc}$) in the case of a $10^8\mathrm{M}_\odot$ BH (left panel) and of a dark cluster with the same mass and 0.2 mas radius.

(MDO). If a MDO with mass $M_\bullet$ is confined in a volume of $4/3\pi(R_{\rm res}/2)^3$, where $R_{\rm res}$ is the spatial resolution of the observations (e.g. the FWHM of the PSF), then it will have an average density of at least $\rho_{\rm BH} > M_\bullet/(4/3\pi(R_{res}/2)^3)$. If the average density is very high then the only possibility is that of a BH because the possible alternative, i.e. a cluster of dark objects, will have a lifetime much shorter than the age of the universe. Unfortunately, as shown by Maoz (1997), only for the Galactic Center and NGC 4258 we can exclude that the MDO is a cluster of dark objects. However, it is still commonly believed that the MDO found in galaxy nuclei are massive BHs.

To summarize the observational evidence suggests that massive BHs are present in all galaxies but only ~ 40 are detected directly, there are a few detections in the 10^7-$10^9\mathrm{M}_\odot$ range, and measurements are limited to the local universe ($D < 100\,\mathrm{Mpc}$). Not all BH detections are equally reliable and, indeed, only for the Milky way and NGC4258 a BH is the only viable possibility. The open questions that we would like to address are the following:

- Do supermassive BHs really exist and are ubiquitous in galaxy nuclei?
- Are there any intermediate mass BHs i.e. $10^3 < M_{\rm BH} < 10^6\mathrm{M}_\odot$?
- When did the relations with the host galaxy set and how do they evolve with time?

We now show how NGOI can be used to detect BHs and measure their masses using gas kinematics. The assumption of the gas kinematical method is to have ionized gas disks rotating under the influence of the central BH and galaxy potential. Of course, one has to take into account the smearing due to the spatial PSF of his observational apparatus.

Let's consider the case of Centaurus A as an example of how we can determine securely whether a massive dark object is a BH. Centaurus A, at a distance of 3.5 Mpc, has a candidate BH with $M_{\rm BH} \sim 10^8\mathrm{M}_\odot$ (Marconi et al. 2001). In Fig. 3 we plot the simulated position velocity diagrams obtained along the major axis of the gas disk rotating around a $10^8\mathrm{M}_\odot$ BH (left panel) or in the gravitational field of a dark cluster with the same mass and a radius of

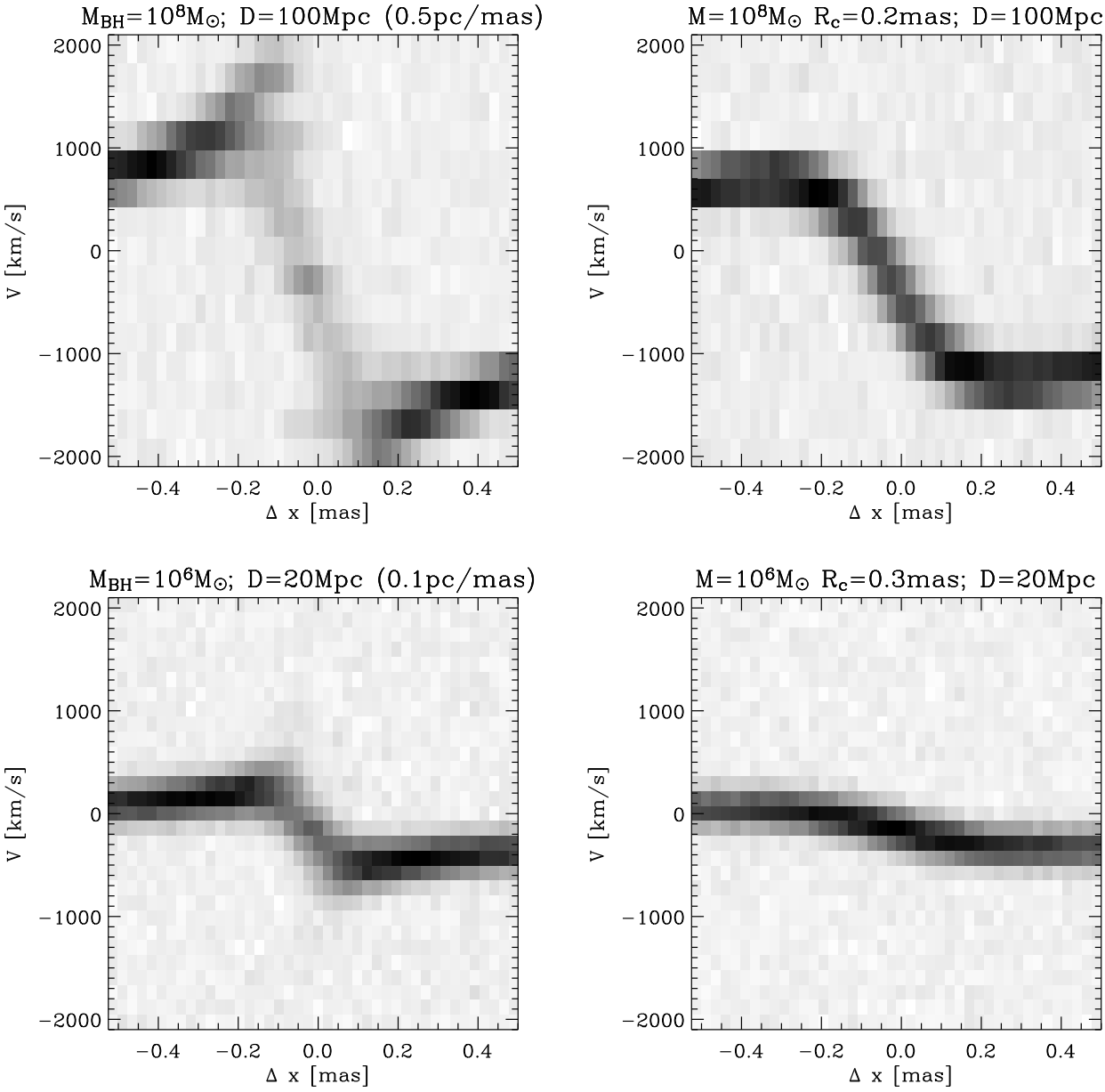

Figure 4: Position velocity diagrams from NGOI observations of BHs (left panels) and of dark clusters with the same mass and 0.2 mas radius. From top to bottom: $M_{\rm BH} = 10^8 {\rm M}_\odot$ at $D = 100\,{\rm Mpc}$ and $M_{\rm BH} = 10^6 {\rm M}_\odot$ at $D = 20\,{\rm Mpc}$.

0.2 mas (right panel). This position velocity diagrams can be obtained from observations of the Brγ 2.18 μm line with a spatial resolution of 0.1 mas (FWHM of the PSF). The field of view is 1x1 mas and is sampled by 0.02x0.02 mas pixels for a total of 50x50 elements. For each spatial pixel a spectrum is available with 300 km/s velocity bins. The contrast achieved in the simulated observations, defined as the strongest feature divided by the 1σ noise, is 100. The two cases, BH or dark cluster, are clearly distinguishable because the latter does not produce the high velocities (3000-4000 $\mathrm{km\,s^{-1}}$) which characterize the BH case. In Fig.4 we consider the cases of a $10^8\mathrm{M}_\odot$ BH at a distance of 100 Mpc and of a $10^6\mathrm{M}_\odot$ BH at 20 Mpc. In both cases, with an observational setup similar to Centaurus A, we can clearly distinguish between a BH and a dark mass extended over 0.2 mas.

Thus, NGOI will be able to constrain the MDO in Centaurus A within, at least, a volume of 0.2 mas radius (i.e. 0.034 pc at the distance of Centaurus A) and with $\rho_{\mathrm{BH}} > 6{\times}10^{11}\mathrm{M}_\odot\,\mathrm{pc}^{-3}$ it will be a better case for a BH than NGC 4258. Indeed, according to Maoz (1997) diagram any dark cluster in Centaurus A will have a lifetime of at most 10^8 yr. The dark cluster with $10^8\mathrm{M}_\odot$ at 100 Mpc will have a lifetime of $\sim 10^{10}$ yr while that of $10^6\mathrm{M}_\odot$ at 20 Mpc will have a lifetime of $\sim 10^9$ yr. In all cases we will have better BH evidences than those currently available, except for the Milky Way BH.

Generalizing the above results, in the local universe ($D < 100$ Mpc) we can detect with high significance (i.e. alternative dark cluster with lifetime less than 1/10 of the age of the universe) BHs with masses larger than $10^6\mathrm{M}_\odot$. At a few Mpc distance we can detect down to $10^5\mathrm{M}_\odot$ BHs with the same significance. If we only want to resolve the BH sphere of influence like it has been done for M87 (one of the best cases after the Milky Way and NGC 4258, Macchetto et al. 1997) then we can get down to $10^3\mathrm{M}_\odot$ BHs at 4 Mpc and, similarly, 10^4 at 10 Mpc. All BHs with $M > 10^8\mathrm{M}_\odot$ will be detected at all redshifts with high significance.

In conclusion, we can verify if MDOs are BHs and we can detect and measure BH masses for intermediate mass BHs up to 100 Mpc. We can build accurate M_{BH}-L/$\sigma_\star$ relations at $z = 0$ and, since we can obtain those relations in the 10^8- $10^{10}\mathrm{M}_\odot$ range at all redhisfts, we can study when those relations set and evolve in massive galaxies.

5 The Broad Line Region

The BLR (Broad Line Region) is the region where the broad (FWHM> 1000 km/s) permitted lines observed in the spectra of type 1 AGNs originate (e.g. Blandford, Netzer & Woltjer 1990). Given the small distance from the central BH the width of the broad lines is likely to originate from the gravitational motion of gas clouds around the BH. So far, the size of the BLR could not be directly measured and the only available information is provided by the so-called reverberation mapping technique (e.g. Peterson 1994). The BLR size is estimated as $c\Delta\tau$ where $\Delta\tau$ is the time lag between the continuum and line variation. Clearly this represents an average size weighted over the BLR geometry and physical conditions. In principle the BLR geometry and kinematics can be derived from the detailed behavior of the light curves, but the inversion is not unique mainly because of the correspondence between the 1-dimensional nature of light curves and the 3-dimensional nature of the BLR. Also the non optimal time sampling of the observations strongly reduces the constraints which can be derived. Suggested spatial distribution of the BLR clouds are spherical, disk-like or conical. Dynamically, the BLR might be dominated by gravitational motions (either a virialized system with chaotic motions or a disk in keplerian rotation), or might be part of a radiation pressure driven outflow, or of an inflow. Obtaining a direct measure of the BLR size and constraining its morphology and kinematics is fundamental in order to understand its origins and relationship with AGN

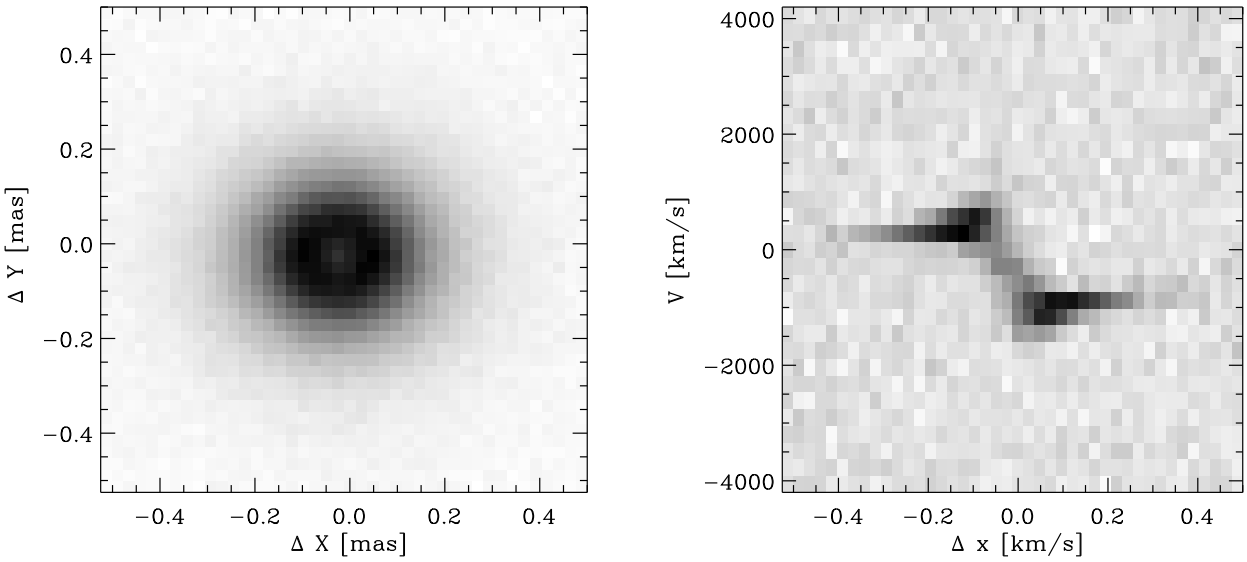

Figure 5: Left: Paα image of the BLR in 3C273 obtained with NGOI. The BLR is assumed to be in a rotating disk. Right: position-velocity diagram extracted along the major axis of the disk (x-axis).

activity, and to measure the mass of the BH and verify reverberation mapping techniques. BLR sizes determined with the reverberation mapping have been found to correlate with the quasar luminosity. A recent estimate by Kaspi et al. 2000 gives:

$$R_{BLR} \sim 33 \left(\frac{\lambda L_\lambda (5100\text{Å})}{10^{44}\, erg\, s^{-1}} \right)^{0.7} \text{light days} \tag{3}$$

where L_λ is the rest-frame monochromatic luminosity at 5100 Å.

Assuming virialized motions, the BH mass can be estimated as

$$M_{\rm BH} = 1.45\, 10^7 {\rm M}_\odot \left(\frac{c\tau_{BLR}}{100 lt-day} \right) \left(\frac{FWHM}{1000\, {\rm km\, s^{-1}}} \right)^2 \tag{4}$$

e.g. Kaspi et al. 2000, Peterson et al. 2004. Potentially reverberation mapping is plagued by so many uncertainties that the question on its reliability arises naturally. However, the best confirmation for reverberation mapping comes from the fact that BH masses estimated with reverberation mapping agree well with the $M_{\rm BH}$-L/$\sigma_\star$ relations found for quiescent galaxies (e.g. Onken et al. 2004). We stress that reverberation mapping is not a direct method to measure BH masses but is calibrated with the $M_{\rm BH}$-L/$\sigma_\star$ relations. Obtaining $R_{\rm BLR}$ from reverberation mapping is observationally extremely expensive because it requires monitoring of a single AGN for a few years. However one can take advantage of the $R_{\rm BLR}$-luminosity relation shown above to easily estimate $R_{\rm BLR}$ from the AGN continuum. The BH mass can then be estimated from the virial relation as $M_{\rm BH} = f R_{\rm BLR} \Delta V^2 / G$ where f is a factor which depends on the geometry of the BLR. This provides an easy and quick method to estimate $M_{\rm BH}$ in thousands of objects at all redshifts. As in the case of reverberation mapping, the reliability of this method lies on the agreement of $M_{\rm BH}$ estimates with the $M_{\rm BH}$-L/$\sigma_\star$ relations.

Given these premises, the open questions which we would like to answer are:

- What are BLR geometry and kinematics?

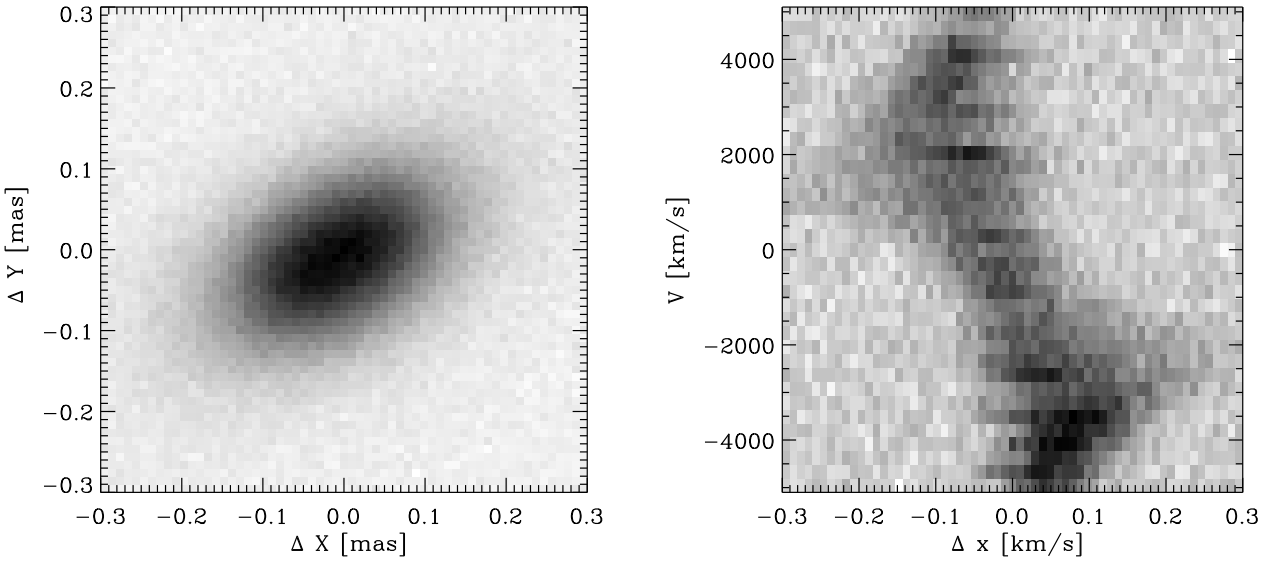

Figure 6: Left: MgII λ2799 image of the BLR in the highest redshift currently known (z = 6.421) obtained with NGOI. The BLR is assumed to be in a rotating disk. Right: position-velocity diagram extracted along the major axis of the disk (30deg off the x-axis).

- How good is the $R_{\rm BLR}$-Luminosity relation and how it extends to high luminosities?
- Is the BLR virialized?
- Are virial mass estimates reliable? Can we improve on their accuracy, e.g. by having more accurate f?

We now show how observations with NGOI can address these questions. First we consider the case of the famous quasar 3C 273. With $z = 0.16$ the projected scale on the sky is 2.76 pc/mas and is possible to study the Paα line redshifted into the K band. From reverberation mapping studies (Kaspi et al. 2000, Peterson et al. 2004), the time lag of emission lines is $\sim$ 300 lt-days, hence $R_{\rm BLR}$=0.25 pc=0.1 mas. The estimated BH mass is $M_{\rm BH}$=2×10^{8}M$_\odot$ and we assume that the BLR is in a rotating disk with 30deg inclination w.r.t. to the line of sight and that the line emissivity scales as $F(r) \sim \exp(-r/R_{\rm BLR})$ with a $R_H = 0.05$ mas hole. In Figure 5, left panel, we show the reconstructed BLR image obtained in the Paα line with NGOI. The spatial resolution of the observations is 1 mas, and the image is made of 40x40 pixels with 0.025 mas/pix. The contrast is 100. In the right panel we show the position velocity diagram extracted along the disk major axis. The spectral bins corresponds to 300 km s^{-1}. As shown in the figure, the BLR of 3C273 is spatially resolved and from the BLR kinematics one can get a direct measure of BH mass.

We now consider the BLR of the highest redshift QSO known whose estimated BH mass is $M_{\rm BH}$=3×10^{9}M$_\odot$ (Willott et al. 2003). It has a K band magnitude of 16.7 and, at $z = 6.41$, the MgII λ 2799 is redshifted to 2.1 μm. From L(3000Å) it is derived $\tau_{\rm BLR} = 520$ lt-days hence $R_{\rm BLR} = 0.4$ pc $= 0.07$ mas (the scale is 5.5 pc/mas) which, combined with a line width of $FWHM = 6000$ km s^{-1}, provides the above BH mass. We assume that the BLR is in a disk with 60 degrees inclination w.r.t. to the line of sight and that $F(r) \sim \exp(-r/R_{\rm BLR})$ with a $R_H = 0.035$ mas hole. In Figure 6, left panel, we show the reconstructed BLR image obtained in the MgII line with NGOI. The spatial resolution of the observations is 1 mas, and the image

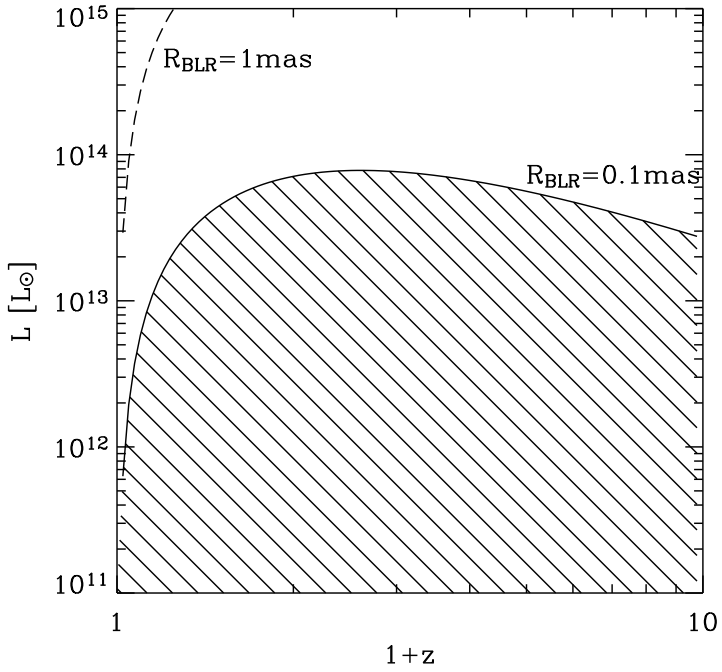

Figure 7: Shaded area: locus in the $L - z$ plane where the BLR radius is $R_{\rm BLR} \leq 0.1\,{\rm mas}$. The dashed line represents the case $R_{\rm BLR} = 1\,{\rm mas}$.

is made of 60x60 pixels with 0.01 mas/pix. The contrast is 50. In the right panel we show the position velocity diagram extracted along the disk major axis. The spectral bins corresponds to $300\,{\rm km\,s^{-1}}$. Like in the case of 3C273, the BLR of the highest redshift quasar is spatially resolved and from its kinematics one can get a direct measure of BH mass.

To generalize the two previous cases, the dashed area in Fig. 7 is the locus in the $L - z$ plane where the BLR radius is $R_{\rm BLR} \leq 0.1\,{\rm mas}$. The dashed line represents the locus where $R_{\rm BLR} = 1\,{\rm mas}$. Therefore, NGOI with the 0.1mas spatial resolution are able to study geometry and kinematics of the BLRs of the brightest quasars at all redshifts. It is also able to study the BLRs of lower luminosity quasars in the local universe. In conclusions, observations of the BLR with NGOI can address all the open questions presented above because it is possible to study morphology and kinematics of the BLR in 10^{12}- 10^{14}L$_\odot$ quasars in the local universe and in 10^{14} quasars at all redshifts.

6 The Obscuring Torus

The nuclear near-IR luminosity of several AGNs is dominated by emission of hot dust, close to the sublimation limit, which traces the inner walls of the circumnuclear molecular torus. The inner radius of the torus is set by the minimum distance from the nuclear UV source at which dust can survive against sublimation, i.e. $R_{Dust\ Subl.} \simeq 0.2 - 4\,L_{46}^{1/2}$pc where L_{46} is the optical-UV luminosity of the AGN in units of 10^{46} erg/s (Laor & Draine 1993). The smallest radius is for large grains and the largest for small grains. Within the torus, the absorbing dust reprocesses the optical-UV primary radiation into the infrared, via heating of the dust grains. Several authors have modeled the infrared spectral energy distribution of AGNs and have shown that, indeed, the nuclear infrared emission can be explained with reprocessing of the nuclear radiation by dust (e.g. Pier & Krolik 1993; Granato & Danese 1994; Efstathiou & Rowan-Robinson 1995). The obscuring dusty medium is expected to extend from the sublimation radius (less than a pc) up to about 100 pc (Granato et al. 1997; Maiolino & Rieke 1995).

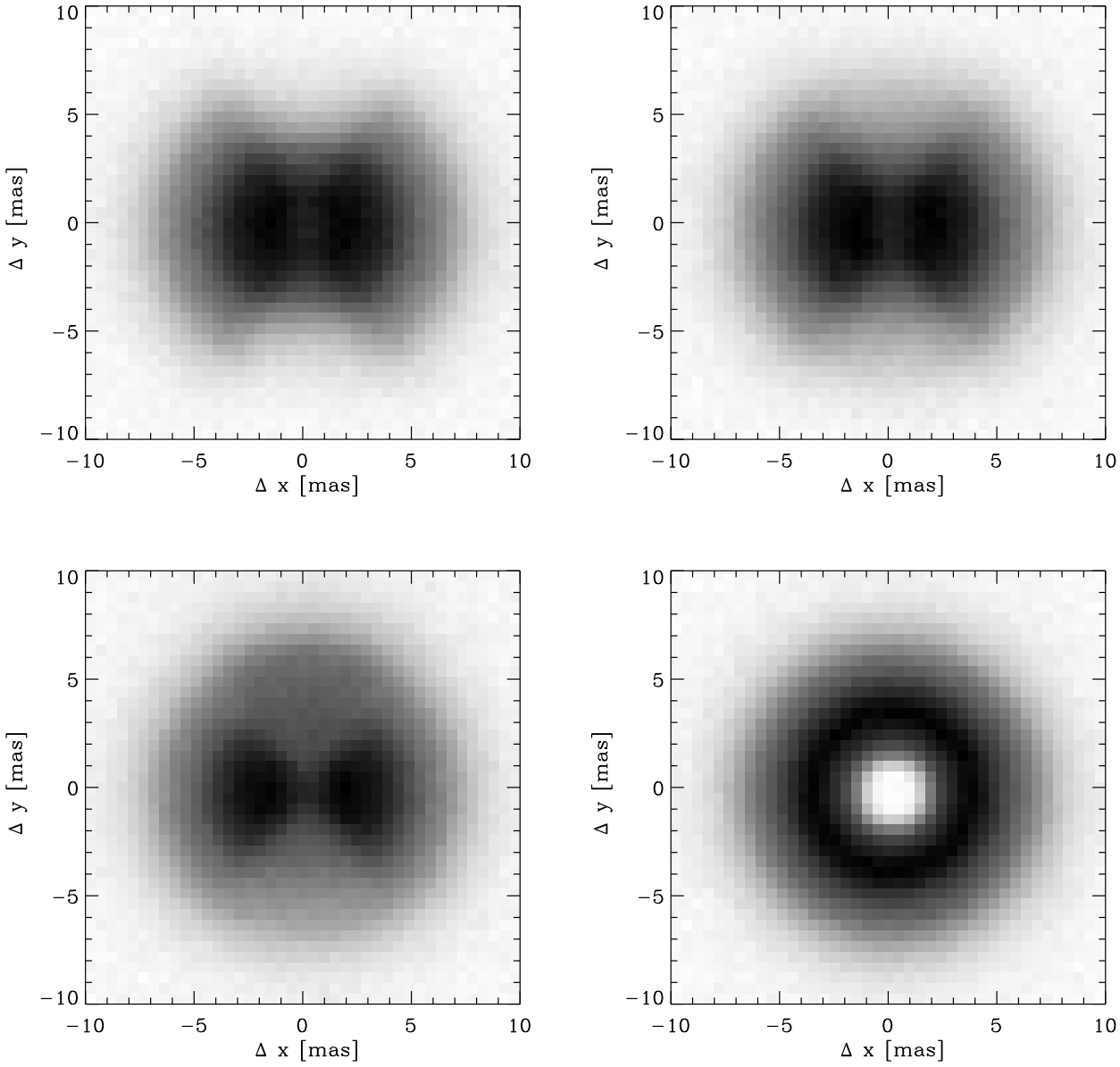

Figure 8: K band images of the obscuring torus of NGC 1068 seen with different inclinations w.r.t. to the line of sight: from left to right i=90, 65 (upper panels), 45, 0 deg (lower panels).

Until a few years ago, the only constraints on the models were the infrared spectral energy distributions and the upper limits on the size of the nuclear H and K band sources obtained from ground-based and HST/NICMOS observations. Without strong constraints on the sizes and geometries of the tori, there is a degeneracy between the model parameters (like dust composition, distribution etc.) meaning that the same spectra and size constraints can be adequately explained with very different torus models. The radiative transfer models have been recently compared with the IR SED of nearby Seyfert galaxies and with high angular resolution near- and mid-IR observations to try to constrain the physics and the geometry of the dusty torus (e.g. Alloin et al. 2000; Maiolino et al. 1998) with the finding that the near- and mid-IR emitting dust is somewhat more extended than expected by the early models. The geometry and the physics of the dusty gas in the circumnuclear region of AGN are thus more complex than assumed so far. An additional complication is that the properties of dust in AGNs might be different with respect to the diffuse interstellar medium. More specifically, Maiolino et al. (2001a,b) have shown that probably the dust in the circumnuclear region of AGNs is biased in favor of large grains, while in all models for the molecular torus a "standard" Galactic dust mixture has been assumed. A distribution of dust biased in favor of large grains would change significantly the distribution of temperatures and also the location of the dust sublimation radius.

Open questions are:

- Does torus really exists?
- What is the geometry of the torus?
- What is the dust composition?

Addressing these questions is a crucial test for the unified model. Currently there are no self-consistent physical models of the torus and it is not clear why the dusty medium is kept inflated with respect to a disk geometry.

Early results from the VLTI with MIDI and VINCI observations on NGC 1068 have shown the presence of a compact pc-scale hot dust component with size increasing with wavelength, as expected (e.g. Jaffe et al. 2004, Wittkowski et al. 2004). MIDI observations have also shown that the silicate absorption feature seen on the hot dust component might have a different dust composition than that of the more extended stuff (Jaffe et al. 2004). Though preliminary, these results show the great potential of high resolution interferometric observations.

We now show how a torus can be imaged by NGOI and how it is possible to study its morphology. To this purpouse we use torus models kindly provided by G.L. Granato (Granato et al. 1998).

We first consider the case of the prototypical Seyfert 2 galaxy NGC1068. In Fig. 8 we show how the torus of NGC1068 would appear if observed with NGOI with a 1 mas spatial resolution. Images have a scale of 0.2 mas/pix and are made of 100x100 pixels. The contrast is 50. The different panels are K band images of the torus seen with different inclinations w.r.t. to the line of sight (from left to right and from top to bottom: i=90, 65, 45, 0 deg). From these figures it is clear that 1 mas spatial resolution is more than adequate to study the morphology of the torus, distinguishing for instance among different inclinations with the line of sight.

We now consider the torus of a QSO with $L = 10^{13} L_{\odot}$ at $z = 3.5$. We use the torus model for NGC 1068 rescaling its dimensions as $L^{0.5}$. At $z = 3.5$ the wavelength 2.2 μm is shifted to 10 μm. The left panels in Fig. 9 show torus images at 10 μm obtained with NGOI with a spatial resolution of 0.5 mas (scaling from a resolution of 0.1 mas at 2 μm). Images have a scale of 0.1 mas/pix and and 20x20 pixels. The contrast is 50. In the upper panels the torus has an

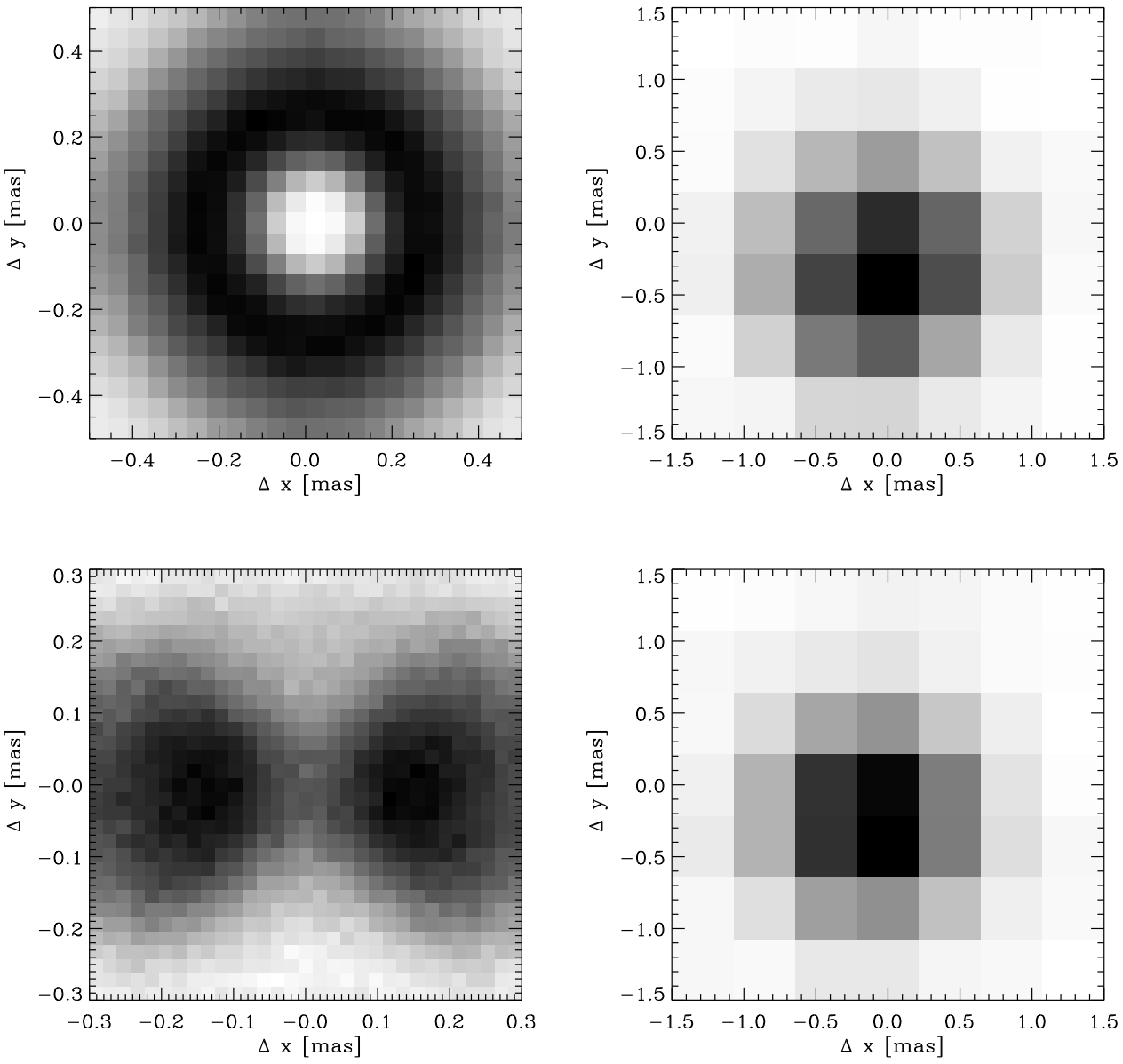

Figure 9: 10μ images of the obscuring torus of a QSO with $L = 10^{13}\mathrm{L}_{\odot}$ at $z = 3.5$ (K band rest frame). Upper panels: the torus has an inclination of 0 deg with respect to the line of sight and is observed with a spatial resolution of 0.1 mas (left) and 1 mas (right). Lower panels: as in the upper panels but the inclination of the torus is 45deg.

inclination of 0 deg while in the lower panels i=45 deg. In the right panels we show the same images but obtained with a spatial resolution of 5 mas (scaling from a resolution of 1 mas at 2 μm). Images have a scale of 0.25 mas/pix and and 7x7 pixels. The contrast is 50. The torus structure can be clearly resolved only in the first case, i.e. with a spatial resolution of 5 mas.

In conclusion, given that the torus size scales as $L^{0.5}$, we can generalize the above results and find that it is possible to study the torus geometry in all AGNs in the local universe. At high redshift, as an example, we can study the torus of a $3\times10^{12}L_{\odot}$ quasar at $z = 0.8$ (rest frame K band is at 4 μm) and the torus of a $10^{13}L_{\odot}$ quasar at $z = 3.5$ (rest frame K band is at 10 μm). We can clearly resolve the torus of the $z = 6$ quasars detected by the SDSS and discussed in the previous section.

7 Conclusions

In the previous sections we have shown that NGOI with the characteristics specified in Sec. 3 can be used to address important open questions on the central Black Hole, on the Broad Line Region and on the Obscuring Torus. In doing so, we have mainly focused on the spatial resolution achievable with NGOI and we have shown that a major step forward can be done with a spatial resolution of 0.1 mas in the K band. The magnitude limits presented in Table 1 guarantee that a large number of AGNs will be observable with NGOI. Of course, to reach those limiting magnitudes observations will require fringe tracking either on-source (type 1 AGNs have strong point-like continuum emission from the accretion disk) or on a nearby star. It is clear that the possibility of performing fringe tracking will be the most severe limitation for the observations described here. NGOI should be able to fringe track on sources down to, at least, $K \sim 18 - 19$ otherwise the scientific goals will be severely limited.

In conclusion, the requirements for the next generation interferometer can be summarized as follows:

- NGOI should have full imaging capabilities which can be achieved with reconstructed images from aperture synthesis.
- Imaging capabilities must be combined with spectral dispersion at low ($\mathcal{R} \sim 50 - 100$ – torus) and medium spectral resolution ($\mathcal{R} = 1000 - 2000$ – BLR and BH).
- The limiting magnitudes should be $K = 22$ ($\mathcal{R} = 50$) and $K = 20$ ($\mathcal{R} = 1000$) in the case of a point source.
- The spatial resolution (in K) should be around 0.1 mas but no worse than 1 mas with the latter value severely limiting the science goals.
- The wavelength range should be 1-2.5 μm but should be extended up to 10 μm in order to study tori at high redshift.
- The field of view should be of the order of 1x1 mas with a pixel size of 0.02-0.05 mas/pix and up to 50x50 elements.
- The achievable contrast should be of the order of 100.
- The fringe tracking should be performed on sources down to $K \sim 18 - 19$ on or off-axis.
- AO correction is needed with artificial or laser stars in order to increase the sky coverage.

With the above requirements in the case of the 0.1 mas resolution NGOI we can achieve the following goals.

Supermassive Black Holes:

- We can verify if MDOs are BHs up to D=100 Mpc.
- We can measure BHs with 10^5-ten6$M_\odot$ masses up to 20 Mpc.
- We can obtain accurate $M_{\rm BH}$-L/$\sigma_\star$ relations at $z = 0$.
- We can study those relations in the 10^8-$10^{10}M_\odot$ mass range at all z and see how they evolve with the age of the universe.

Broad Line Region:

- We can study morphology and kinematics of the BLR of 10^{12}-$10^{13}L_\odot$ quasars in the local universe and of $10^{14}L_\odot$ quasars at all redshifts.

Obscuring torus:

- We can study the geometry of tori in Seyferts in the local universe and in quasars at all redshifts.

If the spatial resolution is limited to 1 mas in K the scientific goals are severely reduced.

Supermassive Black Holes:

- We can verify if MDOs are BHs up to D=10 Mpc.
- We can obtain accurate $M_{\rm BH}$-L/$\sigma_\star$ relations at $z = 0$.

Obscuring torus:

- We can study the geometry of tori in Seyferts and quasars in the local universe.

In this case, no studies on the Broad Line Region are possible.

Acknowledgements

A.M. acknowledge support from INAF *Istituto Nazionale di Astrofisica*.

References

Alloin D., Pantin E., Lagage P. O., Granato G. L., 2000, A&A 363, 926-932
Antonucci R., 1993, ARA&A 31, 473
Barth A. J., Sarzi M., Rix H., Ho L. C., Filippenko A. V., Sargent W. L. W., 2001, ApJ, 555, 685
Bennert N., Falcke H., Schulz H., Wilson A. S., Wills B. J., 2002, ApJ, 574, L105
Blandford R. D., Netzer H., Woltjer L., 1990, in "Active Galactic Nuclei", Saas-Fee Advanced Course 20, Lecture Notes 1990, Springer-Verlag
Efstathiou A., Rowan-Robinson M., 1995, MNRAS 273, 649-661
Laor A., Draine B. T., 1993, ApJ, 402, 441

Ferrarese L., Merritt D., 2000, ApJ, 539, L9
Ferrarese L., Ford H. C., 2004, Space Science Reviews, in press (astro-ph/0411247)
Gebhardt K., et al., 2000, ApJ, 539, L13
Gebhardt K., et al., 2003, ApJ, 583, 92
Genzel R., Pichon C., Eckart A., Gerhard O. E., Ott T., 2000, MNRAS, 317, 348
Ghez A. M., Morris M., Becklin E. E., Tanner A., Kremenek T., 2000, Nature, 407, 349
Granato G. L., Danese L., 1994, MNRAS 268, 235
Granato G. L., Danese L., Franceschini A., 1997, ApJ 486, 147
Ho L. C., Peng C. Y., 2001, ApJ, 555, 650
Kaspi S., Smith P. S., Netzer H., Maoz D., Jannuzi B. T., Giveon U., 2000, ApJ, 533, 631
Kormendy J., Richstone D., 1995, ARA&A, 33, 581
Kormendy J., Gebhardt K., 2001, Proc. of 20th Texas Symposium, 363
Jaffe W., et al., 2004, Natur, 429, 47
Macchetto F., Marconi A., Axon D. J., Capetti A., Sparks W., Crane P., 1997, ApJ, 489, 579
Maiolino R., Rieke G. H, 1995, ApJ 454, 95
Maiolino, R., Krabbe A., Thatte N., Genzel R., 1998, ApJ 493, 650
Maiolino R., Marconi A., Salvati M., et al., 2001a, A&A 365, 28-36
Maiolino R., Marconi A., Oliva E., 2001b, A&A 365, 37-48
Maoz E., 1998, ApJ, 494, L181
Marconi A., Capetti A., Axon D. J., Koekemoer A., Macchetto D., Schreier E. J., 2001, ApJ, 549, 915
Marconi A., et al., 2003, ApJ, 586, 868
Marconi A., Hunt L. K., 2003, ApJ, 589, L21
Marconi A., Maiolino R., Petrov R. G., 2003, Ap&SS, 286, 245
Marconi A., Risaliti G., Gilli R., Hunt L. K., Maiolino R., Salvati M., 2004, MNRAS, 351, 169
Miyoshi M., Moran J., Herrnstein J., Greenhill L., Nakai N., Diamond P., Inoue M., 1995, Natur, 373, 127
Netzer H., Laor A., 1993, ApJ, 404, L51
Onken C. A., Ferrarese L., Merritt D., Peterson B. M., Pogge R. W., Vestergaard M., Wandel A., 2004, ApJ, 615, 645
Peterson B. M., 1994 ASP Conf. Ser. 69, 1
Peterson B. M., et al., 2004, ApJ, 613, 682
Pier E. A., Krolik J. H., 1993, ApJ 418, 673
Schmitt H. R., Donley J. L., Antonucci R. R. J., Hutchings J. B., Kinney A. L., Pringle J. E., 2003, ApJ, 597, 768
Schödel R., et al., 2002, Natur, 419, 694
Shapiro S. L., Teukolsky S. A., 1983, 'Black holes, white dwarfs, and neutron stars: The physics of compact objects', New York, Wiley-Interscience
Soltan A., 1982, MNRAS, 200, 115
Tremaine S., et al., 2002, ApJ, 574, 740
Verolme E. K., et al., 2002, MNRAS, 335, 517
Willott C. J., McLure R. J., Jarvis M. J., 2003, ApJ, 587, L15
Wittkowski M., Kervella P., Arsenault R., Paresce F., Beckert T., Weigelt G., 2004, A&A, 418, L39